In Vivo Pharmacokinetics, Biodistribution and Toxicity of Antibody-Conjugated Gold Nanoparticles in Healthy Mice

Noami Daems[1, 2], Bart Verlinden[3], Karen Van Hoecke[3], Thomas Cardinaels[3, 4], Sarah Baatout[1], Carine Michiels[2], Stéphane Lucas[5], and An Aerts[1, *]

[1] *Radiobiology Research Unit, Interdisciplinary Biosciences, Institute for Environment, Health and Safety, Belgian Nuclear Research Centre (SCK CEN), Boeretang 200, 2400 Mol, Belgium*
[2] *Unité de Recherche en Biologie Cellulaire-Namur Research Institute for Life Sciences, University of Namur, Rue de Bruxelles 61, 5000 Namur, Belgium*
[3] *Radiochemistry Expert Group, Institute for Nuclear Materials Science, Belgian Nuclear Research Centre (SCK CEN), Boeretang 200, 2400 Mol, Belgium*
[4] *Katholieke Universiteit Leuven, Department of Chemistry, Celestijnenlaan 200F, 3001 Leuven, Belgium*
[5] *Research Center for the Physics of Matter and Radiation-Namur Research Institute for Life Sciences, University of Namur, Rue de Bruxelles 61, 5000 Namur, Belgium*

Cetuximab-conjugated gold nanoparticles are known to target cancer cells, but display toxicity towards normal kidney, liver and endothelial cells *in vitro*. In this study, we investigated their pharmacokinetics, biodistribution and toxicity after intravenous administration in healthy mice. Our data showed that these nanoparticles were rapidly cleared from the blood and accumulated mainly in the liver and spleen with long-term retention. Acute liver injury, inflammatory activity and vascular damage were transient and negligible, as confirmed by the liver functionality tests and serum marker analysis. There was no sign of altered liver, kidney, lung and spleen morphology up to 4 weeks post-injection. After 6 months, kidney casts and splenic apoptosis appeared to be more prevalent than in the controls. Furthermore, occasional immune cell infiltration was observed in the lungs. Therefore, we recommend additional *in vivo* studies, in order to investigate the long-term toxicity and elimination of gold nanoparticles after multiple dosing in their preclinical validation as new targeted anti-cancer therapies.

KEYWORDS: Gold Nanoparticles, In Vivo, Toxicity, Biodistribution, Pharmacokinetics, Cetuximab.

INTRODUCTION

Over the last few decades, applications of gold nanoparticles (AuNPs) in nanomedicine have developed extensively due to their unique physicochemical properties. Furthermore, the possibility of modifying the surface of AuNPs with targeting agents strengthens their potential use in the diagnosis, monitoring and treatment of cancer [1, 2]. Our previous studies have shown that AuNPs, coated with poly-allylamine and conjugated to Cetuximab (AuNPs-PAA-Ctxb), successfully targeted cancer cells that were overexpressing the epidermal growth factor receptor (EGFR), both *in vitro* and *in vivo* [3, 4]. Furthermore, AuNPs-PAA-Ctxb selectively radiosensitized

EGFR-overexpressing cancer cells, thus increasing the efficacy of 25 keV/μm proton therapy (3.0 Gy) by 22% [5, 6]. Several studies indicate that the physical interaction between AuNPs and radiation, leading to low-energy electron emission, is unlikely to be the only mechanism responsible for the radiosensitizing property of AuNPs [7, 8]. In fact, it has been demonstrated that AuNPs also exert a direct biological effect on the cells. More specifically, AuNPs caused mitochondrial dysfunction, inhibition of the thioredoxin antioxidant defense system and oxidative stress in various cancer cells, which may predispose these cells to the damaging effects of ionizing radiation [9–12]. Moreover, we recently observed the same biological effects in non-cancerous, human kidney, liver and microvascular endothelial cells exposed to AuNPs-PAA-Ctxb *in vitro*. This indicates a general AuNP cytotoxicity mechanism, which is not cancer cell specific [13].

*Author to whom correspondence should be addressed.
Email: an.aerts@sckcen.be

When administered *in vivo*, the reticuloendothelial system (RES) is able to identify AuNPs as foreign substances that need to be sequestered and eliminated, while the renal system rapidly excretes AuNPs that are smaller than 5.5 nm. Therefore, the kidneys and RES organs, such as the liver, spleen and lungs can encounter a significant proportion of the administered AuNPs [14]. Therefore, although AuNPs hold promise to enhance the effectiveness of cancer radiotherapy, off-target accumulation and the cytotoxicity effects of AuNPs observed in normal cells warrant further investigation with respect to their potential toxicity and immunogenicity *in vivo*.

Several studies have reported on the toxicity of AuNPs *in vivo*, but with conflicting conclusions. Some reports have described how AuNPs can cause acute inflammation, changes in white blood cell levels, changes in liver and kidney functional parameters, emphysema of the lungs and damage to the liver, spleen and kidneys [15–20]. This is in contrast to other studies, which could not detect definite signs of *in vivo* toxicity [21–24]. This apparent discrepancy stems from differences in study set-up, with the administration route and dosage playing a pivotal role. In addition, the size, coating, surface charge and shape of the AuNPs also influenced the biodistribution and toxicity outcome [21, 25, 26].

In this study, we investigated the pharmacokinetics, biodistribution and potential toxicity of our unique, in-house produced AuNPs-PAA-Ctxb in healthy BL6/57 male mice. As previously described, AuNPs-PAA-Ctxb are spherical and negatively charged (-7.04 ± 0.22 mV in cell culture medium, including 10% fetal bovine serum). These nanoparticles, including the gold core and coating, have a diameter of 4–5 nm, but the size increases to 26 nm if the antibody-functionalization is taken into account [13]. At specific time points after intravenous (IV) injection (5 min, 15 min, 30 min, 1 h, 6 h, 24 h, 72 h, 1 week, 4 weeks and 6 months), mice were sacrificed in order to collect their blood, lungs, kidneys, liver and spleen. The biodistribution of the AuNPs-PAA-Ctxb in these tissues was assessed using inductively coupled plasma mass spectrometry (ICP-MS). In addition, the *in vivo* toxicity was evaluated by monitoring the tissue morphology and functional parameters of the liver. Finally, we screened for certain cytokines that are involved in an immune response or specifically linked to cardiovascular damage because of the previously observed sensitivity of human microvascular endothelial cells to AuNPs-PAA-Ctxb [13].

EXPERIMENTAL DETAILS
Chemicals
Cetuximab (Erbitux® 5 mg/ml) was kindly provided by the Sint-Dimpna Hospital (Geel, Belgium). Arabic gum (AG), the aspartate aminotransferase (AST) activity assay kit (MAK055), the alanine transaminase (ALT) activity assay kit (MAK052), the alkaline phosphatase (ALP)

diethanolamine activity kit (AP0100), the gamma glutamyl transferase (GGT) activity colorimetric assay kit (MAK089), hematoxylin, eosin and formalin were purchased from Sigma–Aldrich (Diegem, Belgium). Paraplast Plus was obtained from Leica Microsystems (Diegem, Belgium) and Nembutal was purchased from Ceva Santé Animale N.V. (Brussels, Belgium). Nitric acid (HNO_3), hydrochloric acid (HCl), hydrogen peroxide (H_2O_2) and hydrofluoric acid (HF) were of trace metal grade and purchased from Fisher Scientific (Merelbeke, Belgium). The external calibration and internal standards were prepared using SPEX Certiprep certified standard solutions (Boom B.V., Meppel, The Netherlands).

Gold Nanoparticles and Antibody Conjugation
AuNPs-PAA were produced and conjugated to Cetuximab as previously described [5, 13, 27]. Aliquots of 900 μg of gold were freeze-dried containing 3% AG. Before injection, the AuNPs-PAA-Ctxb were re-suspended in 1 ml of sterile 0.9% NaCl using pulsed sonication (50 W, 30 kHz, 20% amplitude, 0.5 sec pulses).

Animal Study
Healthy adult (8–10 weeks) male C57/Bl6 mice were housed under standard laboratory conditions with a 12:12 hour light/dark cycle and 4–5 animals per cage. Food and water were available *ad libitum*. All animal experiments were approved by the Ethical Committee Animal Studies of Medanex Clinic and conducted in compliance with the European Communities Council Directive of September 22, 2010. Ten groups of 5–6 animals received a single, non-lethal, IV injection of 100 μl of AuNPs-PAA-Ctxb suspension (90 μg of gold). The animals were anesthetized by intraperitoneal administration of 100 μl Nembutal and euthanized by cardiac puncture, which enabled the collection of blood samples at 5 min, 15 min, 30 min, 1 h, 6 h, 24 h, 72 h and 1 week post-injection in EDTA-coated tubes. In addition, the liver, the spleen, the kidneys and the lungs were collected at 6 h, 24 h, 72 h, 1 week, 4 weeks and 6 months post-injection. Control mice received 100 μl of 0.9% NaCl or 3% AG and were euthanized at 6 h, 24 h or 6 months post-injection, as described above. All the animals were randomly assigned to each time point group.

Inductively Coupled Plasma Mass Spectrometry
The liver, spleen, right kidney and right lung intended for ICP-MS analysis were weighed and homogenized using the TissueLyser II (Qiagen, Antwerp, Belgium). Next, 25–75 mg of blood or homogenized tissue was digested in 3 ml concentrated HNO_3 and 1 ml of H_2O_2 for 4 h at 110 °C on a hotplate. The samples were evaporated to incipient dryness, followed by digestion with 4 ml of aqua regia overnight at 110 °C. After evaporation, the dried samples were dissolved in 5–10 ml of 5% (v/v) aqua

regia. Prior to a 2 h UV digestion treatment in a 705 UV digester (Metrohm, Zwijndrecht, Belgium), the samples were spiked with 100 μL of 30% H_2O_2 to initiate radical formation. Finally, 0.05% HF was added to all samples in order to reduce Au memory effects in the ICP-MS introduction system. The gold concentration in the samples was quantified using an XSeriesII quadrupole ICP-MS instrument (ThermoFisher Scientific, Bremen, Germany) using external calibration standards containing 0.5, 1, 2 and 5 ng/mL of gold. Data was collected from 20 ms dwell time per isotope, 200 sweeps per reading, and 5 readings per sample. A rinsing time of 150 s with a solution containing 5% aqua regia and 0.05% HF was included between each sample. The elements Re, Ir, Tl were used as internal standards. The results are expressed as μg of gold per gram of tissue.

Histological Examination

The right medial lobe of the liver, left kidney, left lung and 1/4th of the spleen intended for histological examination were fixed in 10% formalin for 24 h, after which the samples were dehydrated and embedded in paraffin. Seven μm sections were then prepared and stained with hematoxylin and eosin (H&E) according to a standard protocol. Bright-field images were obtained using a Nikon Ti-Eclipse microscope.

Liver Enzyme Activity Measurement and Luminex Analysis

Blood samples intended for liver enzyme activity measurements and luminex analysis were collected at 6 h and 24 h after injection in serum collection tubes. The blood samples were allowed to clot for 30 minutes at room temperature, after which serum was isolated by centrifugation at 10,000 g for 5 min, aliquoted and stored in Eppendorf tubes at −20 °C until analysis. In order to evaluate liver toxicity, the enzyme activity of AST, ALT, GGT and ALP in serum samples was measured. For this purpose, specific assay kits were used according to the manufacturer's instructions. Samples were measured in duplicate and results were expressed as milliunits/ml (mU/ml). In order to evaluate immunotoxicity and cardiovascular damage, serum levels of CCL2, CCL5, CXCL10, EGF, FGF2, GDF-15, ICAM-1, IFNγ, IL-1β, IL-2, IL-4, IL-6, IL-10, PCK9, P-Selectin, TNFα, uPAR were analyzed using a multiplex magnetic bead array (R&D systems). The luminex assay was performed according to manufacturer's instructions. Samples were measured in duplicate using a Luminex 200 and analyzed with xPONENT 3.1 (Luminex Corporation).

Statistical Analysis

Results were reported as a mean ± standard error (SE). One-way ANOVA was used to test for significant differences between the different treated groups and control groups, followed by a Holm-Sidak post-hoc test in order to correct for multiple comparisons. The statistical analyses were performed using Prism 7.02 software. The level of statistical significance is indicated by the number of asterisks as follows: $^*p < 0.05$, $^{**}p < 0.01$, $^{***}p < 0.001$, $^{****}p < 0.0001$.

RESULTS

Blood Clearance

The AuNPs-PAA-Ctxb blood concentration-time curve was fitted by a three-phase exponential decay function, using Origin 2017 (Fig. 1). The pharmacokinetic parameters are summarized in Table I. The maximum Au concentration (C_{max}) in the blood was reached immediately after IV injection (T_{max}). Our data showed that AuNPs-PAA-Ctxb were rapidly eliminated from the blood circulation, leading to a rapid fall in the initial gold concentration. This explains the short initial half-life ($T_{1/2\alpha}$) of 2.3 minutes (i.e., the time required for the Au concentration in the blood to decrease by 50% of its initial value at T_{max} (5 min post-injection)). This fast clearance was followed by a more gradual decline in Au concentration, which was associated with longer half-lives ($T_{1/2\beta}$ and $T_{1/2\gamma}$). After 6 h, 97% of the initial Au concentration was removed from the blood. Since the gold content in the blood was detected until 1 week after injection, an area under the curve (AUC) of 22.3 μg $\cdot$ h $\cdot$ ml^{-1} and an average blood clearance (C_{bl}) of 4.0 ml $\cdot$ h^{-1} were calculated.

Tissue Distribution

In terms of pharmacokinetics, we observed a rapid clearance of the AuNPs-PAA-Ctxb from the blood to the tissues. Sequestration of AuNPs by the RES organs is
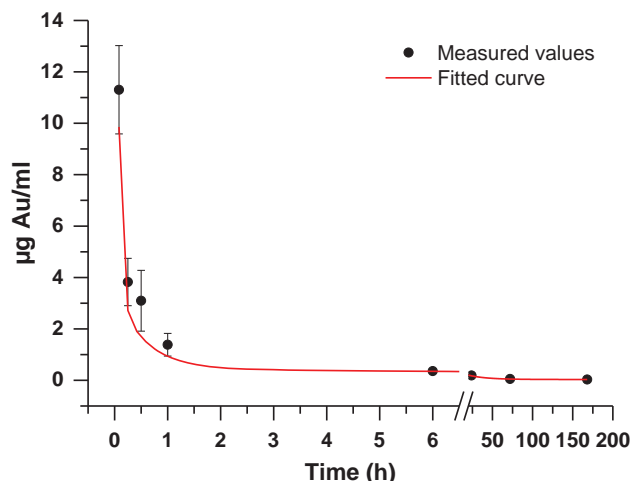

Figure 1. **Blood pharmacokinetic profile of AuNPs-PAA-Ctxb.** Mean gold concentration (μg/ml) in the blood at 5 min, 15 min, 30 min, 1 h, 6 h, 24 h, 72 h and 1 week after a single IV administration (90 μg gold). Error bars represent SE ($n = 5$–6).
Abbreviations: AuNPs-PAA-Ctxb: Gold nanoparticles coated with poly-allylamine and conjugated to Cetuximab; IV: Intravenous; SE: Standard error.

a well-known phenomenon after IV administration [28]. Furthermore, the kidneys can eliminate AuNPs that are smaller than 5.5 nm [14]. Considering the above, we assessed the concentration of AuNPs-PAA-Ctxb using ICP-MS in several RES organs (i.e., liver, spleen, lungs) and the kidneys. Since 97% of the AuNPs-PAA-Ctxb were cleared from the blood circulation after 6 h, AuNPs-PAA-Ctxb distribution was assessed at 6 h, and further monitored at 24 h, 72 h, 1 week, 4 weeks and 6 months post-administration. Figure 2 indicates that AuNPs-PAA-Ctxb accumulated primarily in the liver and the spleen. The gold concentration (μg gold/g tissue) was highest in the spleen, followed by the liver, lung and kidney. However, considering the different sizes of the organs, the percentage of injected dose (%ID) was higher in the
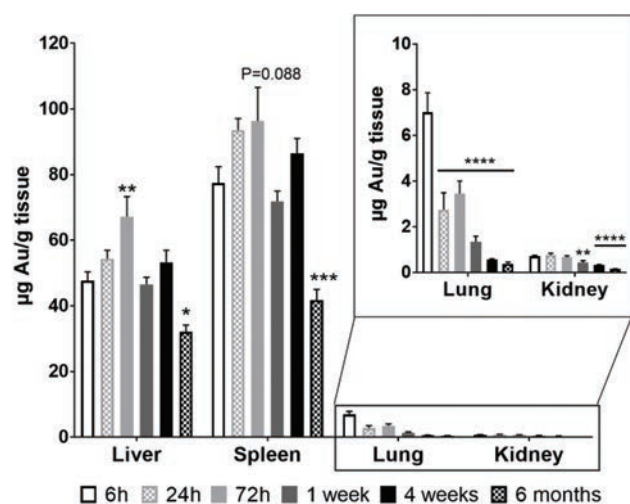

Figure 2. Biodistribution of AuNPs-PAA-Ctxb. Mean gold concentration (μg/g) in liver, spleen, kidney and lung at 6 h, 24 h, 72 h, 1 week, 4 weeks and 6 months after a single IV injection (90 μg gold). Error bars represent SE ($n = 5$–6). The statistical difference compared to 6 h post-injection was calculated by a One-way ANOVA and a Holm-Sidak post-hoc test (*$p < 0.05$, **$p < 0.01$, ***$p < 0.001$ ****$p < 0.0001$).
Abbreviations: AuNPs-PAA-Ctxb: Gold nanoparticles coated with poly-allylamine and conjugated to Cetuximab; IV: Intravenous; SE: Standard error.

liver than in the spleen (Table II). In the liver, the gold concentration significantly increased over time, reaching a maximum value after 72 h (67.24 μg/g). A similar increasing trend in gold concentration was observed in the spleen (maximum after 72 h: 96.34 μg/g). In both liver and spleen, the increase in gold concentration was followed by a significant decline after 6 months (32.11 μg/g liver and 41.76 μg/g spleen). In the lung, the maximum gold concentration was observed after 6 h (7.014 μg/g). This concentration then significantly decreased after 24 h (2.749 μg/g). Finally, the lowest gold concentrations were observed in the kidney (maximum after 24 h: 0.765 μg/g), which significantly decreased after 1 week (0.446 μg/g).

Evaluation of Liver Toxicity

Our biodistribution results showed that a major proportion of the injected AuNPs-PAA-Ctxb accumulated in the liver. Therefore, we evaluated the effect of AuNPs-PAA-Ctxb on the liver by measuring the activity of serum ALT, ALP, AST and GGT. Since 97% of the AuNPs-PAA-Ctxb were distributed to the tissues after 6 h, we assessed acute responses at 6 h and 24 h post-injection. AuNPs-PAA-Ctxb injection led to a small, but significant increase in ALT activity after 6 h, as compared to the arabic gum control group (Fig. 3(A)). Similarly, AST activity significantly increased 6 h after AuNPs-PAA-Ctxb injection, compared to the 0.9% NaCl control group (Fig. 3(B)). In both cases, the increase was transient and undetectable after 24 h. In terms of ALP activity, no significant differences were observed (Fig. 3(C)). Finally, GGT activity was undetectable in all serum samples.

Evaluation of Immunotoxicity and Vascular Damage

The liver and spleen are important lymphoid organs with resident immune cells that can mount a rapid immune response when they encounter antigenic particles. Furthermore, in our previous research, we demonstrated that microvascular endothelial cells were the most sensitive cells to AuNPs-PAA-Ctxb when compared to human kidney and liver cells [13]. Therefore, we measured the serum levels of several markers that are related to inflammatory activity and vascular damage (RANTES, IFNγ, IL-1β, IL-2, IL-4, IL-6, IL-10, TNFα, GDF-15, ICAM-1, CCL2, CXCL-10, P-selectin, PCSK9, uPAR). Since the RES organs rapidly sequestrate the injected AuNPs-PAA-Ctxb, we assessed responses 6 h and 24 h post-injection. No significant increases in serum levels of TNFα, CCL2, IL-1β, IL-2, IL-4, IL-6, IL-10, IFNγ, CXCL-10, PCSK9 and uPAR were observed after administration of AuNPs-PAA-Ctxb (data not shown). On the contrary, serum levels of GDF-15 and P-selectin significantly increased 6 h after AuNPs-PAA-Ctxb injection, as compared to both the 0.9% NaCl and AG control groups. This response was transient and no longer detectable after 24 h (Figs. 4(A–B)).

Table II. Biodistribution of AuNPs-PAA-Ctxb[†]. Gold concentration in liver, spleen, lung and kidney at 6 h, 24 h, 72 h, 1 week, 4 weeks and 6 months after a single IV[‡] injection (90 μg gold) ($n = 5$–6). Results are expressed as the mean %ID[§] $\pm$ SE[ǁ]. The statistical difference compared to 6 h post-injection was calculated by a One-way ANOVA and a Holm-Sidak post-hoc test (*$p <$ 0.05, **$p <$ 0.01, ****$p <$ 0.0001).

| | Theoretically calculated percentage of injected dose (%ID[§]) (mean $\pm$ SE[ǁ]) | | | |
	Liver	Spleen	Lung	Kidney
6 h	50 ± 3	4.5 ± 0.3	0.72 ± 0.07	0.124 ± 0.005
24 h	48 ± 5	5.5 ± 0.4	0.30 ± 0.08****	0.14 ± 0.02
72 h	62 ± 2*	5.5 ± 0.7	0.36 ± 0.06****	0.106 ± 0.009
1 week	52 ± 1	3.9 ± 0.3	0.15 ± 0.02****	0.08 ± 0.01*
4 weeks	47 ± 2	5.5 ± 0.5	0.069 ± 0.007****	0.061 ± 0.005**
6 months	40 ± 3 ($p = 0.058$)	2.4 ± 0.2**	0.045 ± 0.008****	0.033 ± 0.002****

Notes: [†]Gold nanoparticles coated with poly-allylamine and conjugated to Cetuximab, [‡]Intravenous, [§]Percentage of the injected dose, [ǁ]Standard error.

In addition, ICAM-1 levels significantly increased 6 h after AuNPs-PAA-Ctxb injection, as compared to the 0.9% NaCl control group, and remained significantly elevated after 24 h, as compared to both the 0.9% NaCl and AG control groups. It should be noted that a near-significant increase in the ICAM-1 level was also observed 6 h after AG administration, compared to the 0.9% NaCl control

group ($p = 0.051$) (Fig. 4(C)), which was not maintained after 24 h. Finally, the serum level of RANTES significantly increased 6 h after AG administration compared to the 0.9% NaCl control group, but was no longer detected after 24 h (Fig. 4(D)).
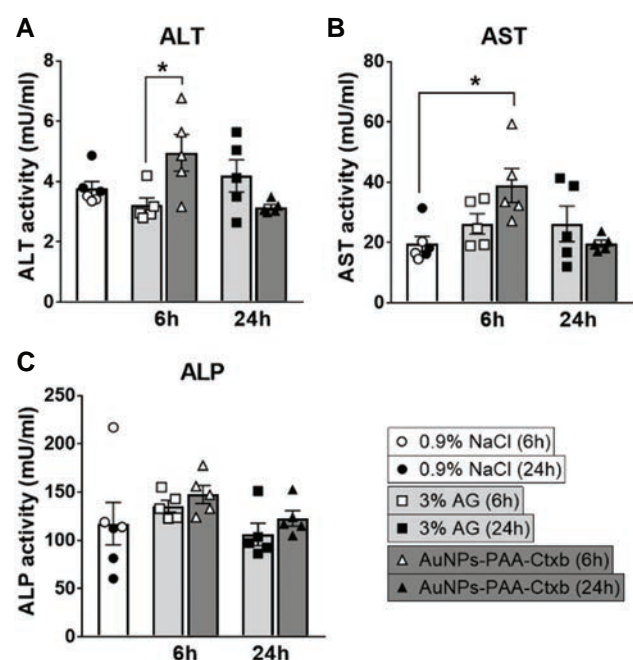

Figure 3. Liver functionality tests. Liver enzyme activity of (A) ALT, (B) AST and (C) ALP in mouse serum at 6 h and 24 h after a single IV injection of AuNPs-PAA-Ctxb (90 μg Au), 0.9% NaCl or AG. Graphs show individual data points and the mean activity (mU/ml) represented by columns. Error bars represent SE ($n = 5$–6). The statistical difference between the treated groups and the 0.9% NaCl control group or the 3% AG control group was calculated by a One-way ANOVA and a Holm-Sidak post-hoc test (*$p < 0.05$).
Abbreviations: AG: Arabic gum; ALP: Alkaline phosphatase; ALT: The alanine transaminase; AST: Aspartate aminotransferase; AuNPs-PAA-Ctxb: Gold nanoparticles coated with poly-allylamine and conjugated to Cetuximab; IV: Intravenous; SE: Standard error.
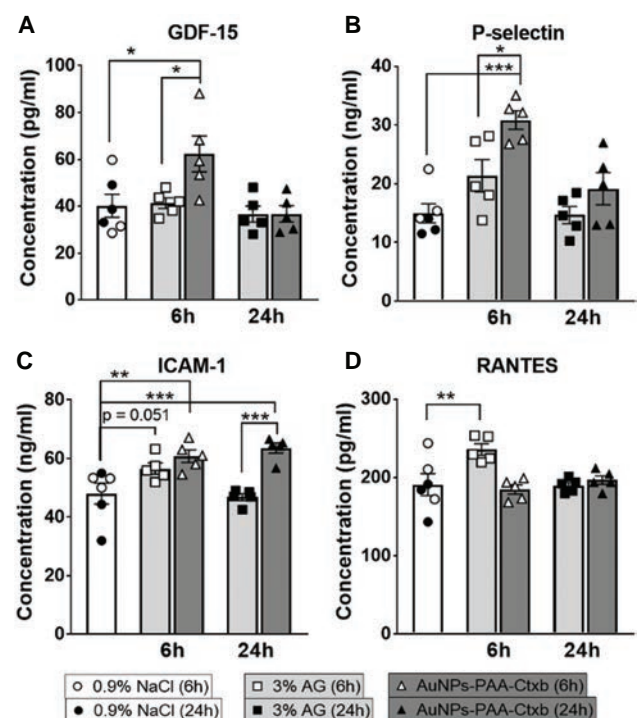
Figure 4. Markers related to inflammatory activity and vascular damage. Serum levels of (A) GDF-15, (B) P-selectin, (C) ICAM-1 and (D) RANTES in mouse serum at 6 h and 24 h after a single IV injection of AuNPs-PAA-Ctxb (90 μg Au), 0.9% NaCl or AG. Graphs show individual data points and the mean concentration (pg or ng/ml) represented by columns. Error bars represent SE ($n = 5$–6). The statistical difference between the treated groups and the 0.9% NaCl control group or the 3% AG control group was calculated by a One-way ANOVA and a Holm-Sidak post-hoc test (*$p < 0.05$, **$p < 0.01$, ***$p < 0.001$).
Abbreviations: AG: Arabic gum; AuNPs-PAA-Ctxb: Gold nanoparticles coated with poly-allylamine and conjugated to Cetuximab; IV: Intravenous; SE: Standard error.
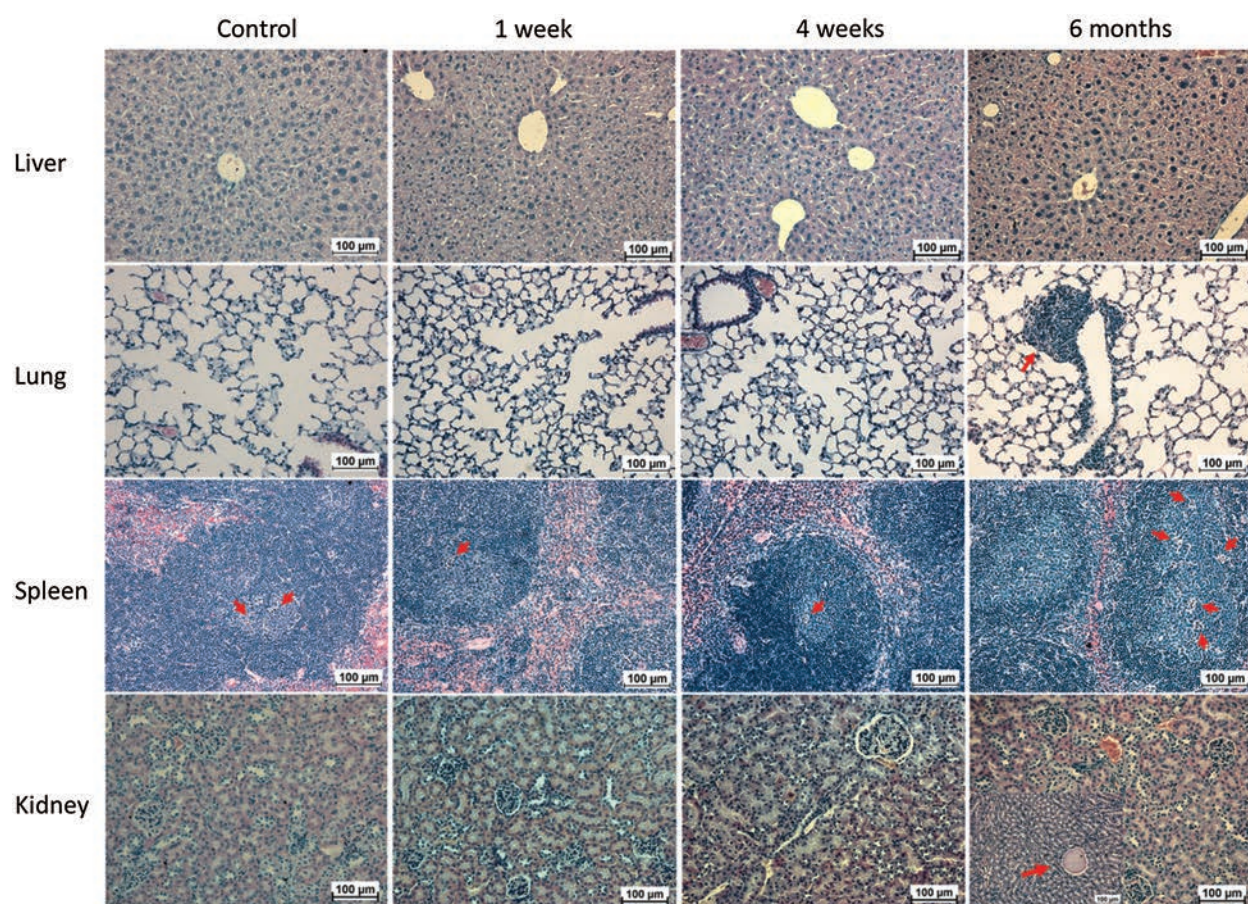
Figure 5. Histological examination. Mouse liver, kidney, spleen and lung at 1 week, 4 weeks and 6 months after a single IV administration of AuNPs-PAA-Ctxb (90 μg Au), compared to the age-related control group, which did not receive AuNPs-PAA-Ctxb. Sections were stained with hematoxylin and eosin. Red arrows indicate immune cell infiltration in the lung, apoptotic cells in the spleen and cast in the collecting tubules of the kidney.
Abbreviations: AuNPs-PAA-Ctxb: Gold nanoparticles coated with poly-allylamine and conjugated to Cetuximab; IV: Intravenous.

Histological Examination

Our biodistribution studies showed that a major proportion of the AuNPs-PAA-Ctxb remained in the liver and spleen 6 months post-injection. Therefore, potential morphological effects of AuNPs-PAA-Ctxb in the organs due to long-term exposure should be considered. Hematoxylin and eosin staining demonstrated normal morphology of the liver (hepatocytes), spleen, kidney (glomeruli and tubules) and lungs (alveoli) 1 week and 4 weeks post-injection (Fig. 5). After 6 months, we observed a modest increase in the number of casts in the collecting tubules of the kidneys (5 out of 6 mice). Furthermore, apoptotic lesions in B-cell rich areas (germinal centers) in the white pulp of the spleen were more noticeable than in the control group (5 out of 6 animals). Finally, some immune cell infiltrations were found in the lungs (4 out of 6 animals). Although the liver accumulated a significant proportion of the injected AuNPs-PAA-Ctxb, no major morphological changes were observed after 6 months.

DISCUSSION

This study focused on the pharmacokinetics, biodistribution and toxicity of our unique in-house produced AuNPs-PAA-Ctxb. The dose was fixed at a single IV injection of 90 μg of gold (7.1×10^{13} AuNPs-PAA-Ctxb). Based on a previous *in vitro* study, in theory, this dose would be sufficient to radiosensitize a small tumor of 11 cm^3 (1.1×10^9 cells) when (1) the dose is extrapolated to a person weighing 60 kg and (2) taking into account that 0.7% of the injected dose would reach the tumor [3–5, 14, 29]. In addition, this dose corresponds to the standard dose range used in most studies, which allows us to compare our results with various *in vivo* studies [26]. The pharmacokinetic data indicated that the AuNPs-PAA-Ctxb were promptly eliminated from the blood stream with a short half-life of 2.3 minutes. This was followed by a predominant accumulation in the liver and spleen, and only a minor uptake in the kidneys and lungs. This observation is similar to the results of a recent study investigating laser-ablated, dextran-coated AuNPs, which had a diameter of 21 nm

and were negatively charged. The authors demonstrated an initial blood half-life of 4.2 minutes and identified the liver and spleen as preferential sites for gold accumulation [30]. The pharmacokinetic results and biodistribution are partly related to the nanoparticle zeta potential and administration mode. Intravenous administration of nanoparticles is typically characterized by the fast adsorption of proteins to the nanoparticle surface, creating a biological identity that is presented to the cells. Charged AuNPs have been shown to adsorb more and a wider variety of proteins than neutral AuNPs. The formation of this protein corona strongly affects the AuNP biodistribution and biological impacts. For instance, adsorption of opsonins, such as complement factors, fibrinogen and IgG antibodies promotes the recognition of nanoparticles by the RES [31]. Since our AuNPs-PAA-Ctxb are negatively charged (-7.04 ± 0.22 mV in cell culture medium including 10% fetal bovine serum), opsonization is likely to occur, leading to the subsequent uptake by phagocytic cells that are in direct contact with the blood and present in the liver and spleen. Nevertheless, IV delivery is a realistic exposure scenario for AuNPs intended to be used in nanomedicine because it resists proteolytic degradation, achieves maximum bioavailability of the drug and allows fast onset of action [32]. Other administration routes investigated in literature are oral and intraperitoneal administration. Oral administration of AuNPs is usually associated with low systemic absorption and high gastro-intestinal elimination [33–36], whereas intraperitoneal administration is followed by retention in the peritoneal cavity, delayed and reduced accumulation in the liver and spleen, and uptake in the pancreas, lungs, lymph nodes and intestine [37–40]. Subcutaneous administration of AuNPs has been used to visualize sentinel lymph nodes [41].

The rapid sequestration by the RES after IV administration could potentially be delayed by modifying the surface of AuNPs with nonionic, sterically stabilizing hydrophilic polymers, such as polyethylene glycol (PEG). This would neutralize the surface charges of AuNPs, shield them from opsonization, and therefore prolong their blood circulation half-life [15, 28, 42–50]. Furthermore, predominant accumulation in the liver and spleen increases as the particle size increases, whereas small AuNPs (1.4–10 nm) have a wider organ distribution profile, with particles detected in the brain, heart, uterus, testis, thymus, kidneys and lungs [28, 51–53]. It is possible that the size of our AuNPs-PAA-Ctxb (26 nm), together with a negative surface charge, favors their uptake by the liver and spleen after IV injection.

Interestingly, although 97% of the injected AuNPs-PAA-Ctxb were cleared from the blood after 6 h, an increasing trend in gold concentration was observed in the liver and spleen for up to 72 h post-injection. Comparable results were obtained with PEGylated AuNPs of different sizes (6.2 nm–61.2 nm) or with different shapes (rods and triangles) reaching maximum gold concentrations in the liver and spleen between 24 h and 6 days post-injection [54, 55]. This increase could potentially be attributed to a gradual redistribution of AuNPs-PAA-Ctxb from other tissues to the liver and spleen [22]. Furthermore, with a diameter of approximately 26 nm and a negative surface charge, AuNPs-PAA-Ctxb are less likely to be efficiently excreted by the negatively charged glomeruli, thus allowing redistribution to occur [25]. This is consistent with our biodistribution data illustrating the lowest amount of gold in the kidneys. In contrast to the liver and spleen, the gold concentration in the lungs and kidneys did not initially increase, but instead progressively decreased after 24 h and 1 week, respectively.

After sequestration in the liver and spleen, AuNPs-PAA-Ctxb showed a long-term retention, with their concentration significantly decreasing only after 6 months. This indicates a slow elimination process, which has also been reported by several other long-term biodistribution studies [21, 25, 55–57]. In addition, it was reported that negatively charged particles were retained for slightly longer in the liver and spleen, and were eliminated more slowly compared to positively or neutrally charged particles [25, 51]. The phagocytic cells in the RES system are responsible for recognizing and clearing AuNPs after IV administration [28]. Sadauskas et al. investigated what happens to negatively charged 40 nm AuNPs in the liver and revealed that they were clustered inside endosome-like vesicles in long-living Kupffer cells, over a period of 6 months, and that damaged cells were cleared by new or nearby Kupffer cells [56]. The presence of PEGylated AuNPs in intracellular vesicles was also confirmed in splenic macrophages [15, 55]. In addition, a recent study demonstrated that the depletion of Kupffer cells greatly improved the elimination efficiency of PEGylated AuNPs. Furthermore, ultra-small 4 nm AuNPs underwent a more efficient hepatobiliary elimination than larger particles, because they were less efficiently captured by the Kupffer cells and had a greater chance of moving from the liver endothelium to the hepatocytes [58]. According to our pharmacokinetic and biodistribution data and the above studies, we could assume that the characteristics of our AuNPs-PAA-Ctxb promote their rapid sequestration by the Kupffer cells and splenic macrophages after IV administration. The clearance of the AuNPs-PAA-Ctxb by these cells protects the organism from exposure to AuNPs-PAA-Ctxb and their related metabolites. However, it also prevents efficient nanoparticle elimination from the body, which explains their long-term retention. Although the elimination pathways are not assessed in this research, significant reduction of the gold concentration in the liver after 6 months could potentially result from occasional lysosomal damage and macrophage cell death, induced by the non-biodegradable AuNPs [59]. Subsequently, the hepatocytes could internalize some of the released AuNPs, thus

leading to gradual and slow elimination via the hepatobiliary pathway [28, 56]. Renal elimination of AuNPs-PAA-Ctxb is less likely, due to their size and negative surface charge, as mentioned earlier. The localization of a small amount of AuNPs-PAA-Ctxb in lungs and kidneys is less clear, but resident alveolar and kidney macrophages could be involved.

Since the AuNPs-PAA-Ctxb were rapidly removed from the blood circulation and mainly sequestered by the liver, we were interested in the effects of AuNPs-PAA-Ctxb on the liver. Therefore, we investigated the activity of the liver enzymes ALT, ALP, AST and GGT in serum 6 h and 24 h post-injection. GGT activity was undetectable in all serum samples, and ALP activity was not significantly different from the control groups. This suggests that there was no obstruction of the biliary tract. However, AST and ALT activities (characteristic for hepatocellular injury) were significantly increased 6 h after AuNPs-PAA-Ctxb injection, compared to the 0.9% NaCl or AG control groups, respectively. These increases were no longer detectable after 24 h. Since the ALT and AST increases were minimal (1.5 and 2 times, respectively) we should question whether the statistically significant differences were also biologically and toxicologically relevant. In comparison, a toxic dose of acetaminophen, which results in severe liver injury, can increase the serum ALT and AST activities to several hundreds to thousands U/L in mice and rats, 4–12 h after administration. These activities can increase further after 24 h [60, 61]. Therefore, if the AST and ALT activity increases in our study were indeed biologically relevant, then the AuNPs-PAA-Ctxb-induced stress to the liver was only mild and transient. Several other studies observed no significantly elevated liver enzyme activities up to 90 days after AuNPs administration compared to the controls [21–23, 25, 30, 49, 62–65]. Injection of 3% AG did not significantly affect the enzyme activities compared to the 0.9% NaCl controls, indicating that AG does not lead to hepatic injury.

In our previous *in vitro* study, microvascular endothelial cells were shown to be the most sensitive cells to AuNPs-PAA-Ctxb, compared to human kidney and liver cells. Therefore, we investigated the serum levels of specific cytokines related to vascular damage and inflammatory activity. Out of all the cytokines that we investigated (RANTES, IFNγ, IL-1β, IL-2, IL-4, IL-6, IL-10, TNFα, GDF-15, ICAM-1, CCL2, CXCL-10, P-selectin, PCSK9, uPAR), only the serum levels of GDF-15, P-selectin and ICAM-1 significantly increased 6 h after AuNPs-PAA-Ctxb administration, when compared to the 0.9% NaCl and AG control groups. For GDF-15 and P-selectin, the increases were transient and no longer detectable after 24 h. The serum level of ICAM-1 remained elevated after 24 h. It should be noted that ICAM-1 was also near-significantly elevated 6 h after AG injection, when compared to the 0.9% NaCl control group. Unlike

after AuNPs-PAA-Ctxb injection, ICAM-1 level was no longer increased 24 h after AG injection. Therefore, we could suggest that AG might transiently increase ICAM-1 expression, which could be enhanced and prolonged by AuNPs-PAA-Ctxb. Finally, the chemokine RANTES was significantly elevated 6 h after AG administration, compared to the 0.9% NaCl control group. However, this was not observed 6 h after AuNPs-PAA-Ctxb administration, which questions the biological relevance of the increase or indicates that AuNPs-PAA-Ctxb eliminated the effect of AG on RANTES expression. GDF-15, P-selectin and ICAM-1 have been identified as biomarkers that reflect acute inflammation, endothelial cell activation and the recruitment of leukocytes to the vessel wall [66]. However, the increases associated with these markers in this study were slight and mostly transient. Furthermore, levels of none of the other pro-inflammatory cytokines were significantly elevated. Based on these findings, we could propose that the risk of vascular damage and any acute immune response elicited by our AuNPs-PAA-Ctxb is limited. In the literature, different outcomes on immunoreactivity after AuNPs administration were identified. For example, liver mRNA levels of several adhesion molecules (ICAM-1, E-selectin and VCAM-1), chemokines (CCL-2, CCL-3, MIP-1β and RANTES) and inflammatory cytokines (IL-1β, IL-6, IL-10, IL-12β and TNFα) were transiently elevated 30 min to 24 h after administration of AuNPs, which suggests the presence of an acute immune response [15, 67]. In contrast, various other studies observed no significant differences in hematological white blood cell indices and TNF-α, IL-1β, IL-6 and IL-10 levels after AuNPs administration [21–23, 30, 49, 63–65, 68]. Interestingly, a study focusing on the effects of antibody-conjugated AuNPs on the vascular system found that IV injection of AuNP-IgG even suppressed leukocyte adhesion to vessel walls. Furthermore, AuNPs-IgG prevented the expression of adhesion molecule PECAM-1, chemotaxis and oxidative stress activation on neutrophils after stimulation, which suggests an anti-inflammatory effect [69].

Finally, since the AuNPs-PAA-Ctxb had a slow excretion rate from the body, we performed histological examinations at 1 week, 4 weeks and 6 months after injection. We did not observe any signs of toxicity until 4 weeks post-injection. Consistent with our results, other studies showed normal organ morphology without apoptosis, necrosis and fibrosis until 90 days after AuNPs administration [21–23, 25, 30, 49, 55, 64]. However, at 6 months post-injection, we were able to observe a slightly increased presence of (1) immune cell infiltrations in the lung, (2) apoptotic lesions in the germinal center and white pulp of the spleen, and (3) casts in the collecting tubules of the kidney. Importantly, apoptotic lesions in the germinal center of the spleen and casts in the kidney were also occasionally observed in the control group, but

from the qualitative images obtained, they seemed to be more noticeable 6 months after AuNPs-PAA-Ctxb injection. Comparable histological observations of the spleen and kidneys were reported previously. However, these results were obtained 1 week after injection [70]. The origin of the kidney casts in our study are unclear. In the spleen, the apoptotic lesions were mostly characterized by the presence of tangible body macrophages (TBMs), which are responsible for the clearance of apoptotic lymphocytes and required to down-regulate the germinal center reaction. This could suggest a potential activity of the adaptive immune response [71]. Interestingly, although a major proportion of the AuNPs-PAA-Ctxb accumulated in the liver, no histological abnormalities were observed until 6 months post-injection, which suggests organ-specific sensitivity to AuNPs-PAA-Ctxb. This is not consistent with another study, which shows increased apoptosis in the liver 1 week after IV injection of 4.26 mg/kg 13 nm PEG-coated AuNPs [15].

Overall, from our functional and morphological observations, and since all the mice survived, showing normal behavior and appearance over the course of the experiment, we consider the toxicity of our AuNPs-PAA-Ctxb to be reasonably low. These results could be related to the surface charge and administration mode, which can affect the toxicity profile of the AuNPs. In fact, a study by Zhang et al. demonstrated that intravenous injection of 13.5 nm AuNPs showed the lowest toxicity compared to the intraperitoneal and oral administration routes, which caused a significant decrease in body weight, spleen index and hematocrit [72]. Furthermore, in general, positively charged AuNPs exhibit a higher cytotoxicity profile than their negatively charged counterparts. Usually, this difference is associated with the electrostatic attraction and adhesion of the positively charged AuNPs to the negatively charged cell membrane, causing depolarization of the plasma membrane and disruption of the membrane integrity [73, 74]. Wang et al. confirmed that the AuNP surface charge influences the toxicity in healthy mice, with 3 mM of positively charged gold nanoclusters (3.7 nm) inducing the most prominent effects on the peripheral blood system, compared to neutral and negatively charged gold nanoclusters [25]. Similarly, in zebrafish embryos, positively charged AuNPs (0.8–1.5–15 nm) were lethal at exposure concentrations higher than 400 ppb, whereas the negatively charged AuNPs induced sub-lethal toxic effects. Neutral AuNPs caused no adverse biological response up to a concentration of 50 ppm [75]. Nevertheless, we are not able to exclude long-term toxicity of AuNPs-PAA-Ctxb with certainty. Therefore, we recommend future research, which focuses on *in vivo* AuNPs toxicity, to consider long-term measurements beyond 6 months, including experiments assessing kidney functionality, liver functionality and immunoreactivity. Furthermore, this study was performed after a single IV injection. In a clinical setting,

the use of AuNPs as radiosensitizing agents may require multiple injections. In fact, multiple intravenous injections resulted in a cumulative increase in AuNPs concentration at the tumor site in Swiss nude mice [76]. It should be noted that multiple dosing did not cause adverse effects in normal tissue, as demonstrated by several other studies [49, 70, 77].

CONCLUSIONS

In conclusion, this study describes the pharmacokinetics, biodistribution and toxicity of our in-house produced AuNPs-PAA-Ctxb after a single IV injection. We demonstrated that the acute toxicity of AuNPs-PAA-Ctxb on the liver and vasculature, tested as increased serum AST and ALT activities, and elevated serum levels of GDF-15, P-selectin, ICAM-1 and RANTES, was limited and transient. However, the rapid clearance of the AuNPs-PAA-Ctxb from the blood, sequestration by the liver and spleen and long-term retention of the AuNPs-PAA-Ctxb in these organs could be limiting factors for the use of AuNPs-PAA-Ctxb as radiosensitizing agents *in vivo*. In order to evaluate the radiosensitizing potential of AuNPs-PAA-Ctxb, we are currently labeling the nanoparticles with ^{177}Lu, which allows real-time assessment of the nanoparticle distribution and elimination in tumor-bearing animals. Since splenic apoptosis, kidney casts and immune cell infiltration in the lungs appeared to be more noticeable at 6 months post-injection compared to the controls, we could not exclude long-term toxicity with certainty. Therefore, we recommend that future *in vivo* studies consider long-term toxicity and the elimination of AuNPs after multiple dosing, in their preclinical validation as new targeted anti-cancer therapies.

Conflict of Interest
The authors declare no conflict of interest.

REFERENCES
1. Sztandera, K., Gorzkiewicz, M. and Klajnert-Maculewicz, B., **2019**. Gold nanoparticles in cancer treatment. *Molecular Pharmaceutics*, 16(1), pp.1–23.

2. Popovtzer, R., **2014**. Biomedical applications of gold nanomaterials. *Nanomedicine (London, England), 9*(13), pp.1903–1904.

3. Marega, R., Karmani, L. and Flamant, L., **2012**. Antibody-functionalized polymer-coated gold nanoparticles targeting cancer cells: An in vitro and in vivo study. *Journal of Materials Chemistry, 22*(39), pp.21305–21312.

4. Karmani, L., Labar, D., Valembois, V., Bouchat, V., Nagaswaran, P.G., Bol, A., Gillart, J., Leveque, P., Bouzin, C., Bonifazi, D., Michiels, C., Feron, O., Gregoire, V., Lucas, S., Vander Borght, T. and Gallez, B., **2013**. Antibody-functionalized nanoparticles for imaging cancer: Influence of conjugation to gold nanoparticles on the biodistribution of 89Zr-labeled cetuximab in mice. *Contrast Media & Molecular Imaging, 8*(5), pp.402–408.

5. Li, S., Bouchy, S., Penninckx, S., Marega, R., Fichera, O., Gallez, B., Feron, O., Martinive, P., Heuskin, A.C., Michiels, C. and Lucas, S., **2019**. Antibody-functionalized gold nanoparticles as tumor-targeting radiosensitizers for proton therapy. *Nanomedicine (London, England), 14*(3), pp.317–333.

6. Li, S., Penninckx, S., Karmani, L., Heuskin, A.C., Watillon, K., Marega, R., Zola, J., Corvaglia, V., Genard, G., Gallez, B., Feron, O., Martinive, P., Bonifazi, D., Michiels, C. and Lucas, S., **2016**. LET-dependent radiosensitization effects of gold nanoparticles for proton irradiation. *Nanotechnology, 27*(45), Article No: 455101.

7. Sotiropoulos, M., Henthorn, N.T., Warmenhoven, J.W., Mackay, R.I., Kirkby, K.J. and Merchant, M.J., **2017**. Modelling direct DNA damage for gold nanoparticle enhanced proton therapy. *Nanoscale, 9*(46), pp.18413–18422.

8. Heuskin, A.C., Gallez, B., Feron, O., Martinive, P., Michiels, C. and Lucas, S., **2017**. Metallic nanoparticles irradiated by low-energy protons for radiation therapy: Are there significant physical effects to enhance the dose delivery? *Medical Physics, 44*(8), pp.4299–4312.

9. Penninckx, S., Heuskin, A.C., Michiels, C. and Lucas, S., **2018**. The role of thioredoxin reductase in gold nanoparticle radiosensitization effects. *Nanomedicine (London, England), 13*(22), pp.2917–2937.

10. Penninckx, S., Heuskin, A.C., Michiels, C. and Lucas, S., **2019**. Thioredoxin reductase activity predicts gold nanoparticle radiosensitization effect. *Nanomaterials (Basel), 9*(2), Article No: 295.

11. Taggart, L.E., McMahon, S.J., Currell, F.J., Prise, K.M. and Butterworth, K.T., **2014**. The role of mitochondrial function in gold nanoparticle mediated radiosensitisation. *Cancer Nanotechnology, 5*(1), Article No: 5.

12. Wang, H., Bouzakoura, S., De Mey, S., Jiang, H., Law, K., Dufait, I., Corbet, C., Verovski, V., Gevaert, T., Feron, O., Van Den Berge, D., Storme, G. and De Ridder, M., **2017**. Auranofin radiosensitizes tumor cells through targeting thioredoxin reductase and resulting overproduction of reactive oxygen species. *Oncotarget, 8*(22), pp.35728–35742.

13. Daems, N., Penninckx, S., Nelissen, I., Van Hoecke, K., Cardinaels, T., Baatout, S., Michiels, C., Lucas, S. and Aerts, A., **2019**. Gold nanoparticles affect the antioxidant status in selected normal human cells. *International Journal of Nanomedicine, 14*, pp.4991–5015.

14. Wilhelm, S., Tavares, A.J., Dai, Q., Ohta, S., Audet, J., Dvorak, H.F. and Chan, W.C.W., **2016**. Analysis of nanoparticle delivery to tumours. *Nature Reviews Materials, 1*, Article No: 16014.

15. Cho, W.S., Cho, M., Jeong, J., Choi, M., Cho, H.Y., Han, B.S., Kim, S.H., Kim, H.O., Lim, Y.T., Chung, B. H. and Jeong, J., **2009**. Acute toxicity and pharmacokinetics of 13 nm-sized PEG-coated gold nanoparticles. *Toxicology and Applied Pharmacology, 236*(1), pp.16–24.

16. Zhang, X.D., Wu, D., Shen, X., Liu, P.X., Yang, N., Zhao, B., Zhang, H., Sun, Y.M., Zhang, L.A. and Fan, F.Y., **2011**. Size-dependent in vivo toxicity of PEG-coated gold nanoparticles. *International Journal of Nanomedicine, 6*, pp.2071–2081.

17. Abdelhalim, M.A. and Jarrar, B.M., **2011**. Renal tissue alterations were size-dependent with smaller ones induced more effects and related with time exposure of gold nanoparticles. *Lipids in Health and Disease, 10*, Article No: 163.

18. Abdelhalim, M.A. and Jarrar, B.M., **2011**. Gold nanoparticles induced cloudy swelling to hydropic degeneration, cytoplasmic hyaline vacuolation, polymorphism, binucleation, karyopyknosis, karyolysis, karyorrhexis and necrosis in the liver. *Lipids in Health and Disease, 10*, Article No: 166.

19. Chen, Y.S., Hung, Y.C., Liau, I. and Huang, G.S., **2009**. Assessment of the in vivo toxicity of gold nanoparticles. *Nanoscale Research Letters, 4*(8), pp.858–864.

20. Terentyuk, G.S., Maslyakova, G.N., Suleymanova, L.V., Khlebtsov, B.N., Kogan, B.Y., Akchurin, G.G., Shantrocha, A.V., Maksimova, I.L., Khlebtsov, N.G. and Tuchin, V.V., **2009**. Circulation and distribution of gold nanoparticles and induced alterations of tissue morphology at intravenous particle delivery. *Journal of Biophotonics, 2*(5), pp.292–302.

21. Yang, L., Kuang, H., Zhang, W., Aguilar, Z.P., Wei, H. and Xu, H., **2017**. Comparisons of the biodistribution and toxicological examinations after repeated intravenous administration of silver and gold nanoparticles in mice. *Scientific Reports, 7*(1), Article No: 3303.

22. Naz, F., Koul, V., Srivastava, A., Gupta, Y.K. and Dinda, A.K., **2016**. Biokinetics of ultrafine gold nanoparticles (AuNPs) relating to redistribution and urinary excretion: A long-term in vivo study. *Journal of Drug Targeting, 24*(8), pp.720–729.

23. Lasagna-Reeves, C., Gonzalez-Romero, D., Barria, M.A., Olmedo, I., Clos, A., Sadagopa Ramanujam, V.M., Urayama, A., Vergara, L., Kogan, M.J. and Soto, C., **2010**. Bioaccumulation and toxicity of gold nanoparticles after repeated administration in mice. *Biochemical and Biophysical Research Communications, 393*(4), pp.649–655.

24. Lopez-Chaves, C., Soto-Alvaredo, J., Montes-Bayon, M., Bettmer, J., Llopis, J. and Sanchez-Gonzalez, C., **2018**. Gold nanoparticles: Distribution, bioaccumulation and toxicity. In vitro and in vivo studies. *Nanomedicine: Nanotechnology, Biology, and Medicine, 14*(1), pp.1–12.

25. Wang, J.Y., Chen, J., Yang, J., Wang, H., Shen, X., Sun, Y.M., Guo, M. and Zhang, X.D., **2016**. Effects of surface charges of gold nanoclusters on long-term in vivo biodistribution, toxicity, and cancer radiation therapy. *International Journal of Nanomedicine, 11*, pp.3475–3485.

26. Khlebtsov, N. and Dykman, L., **2011**. Biodistribution and toxicity of engineered gold nanoparticles: A review of in vitro and in vivo studies. *Chemical Society Reviews, 40*(3), pp.1647–1671.

27. Moreau, N., Michiels, C., Masereel, B., Feron, O., Gallez, B., Vander Borght, T. and Lucas, S., **2009**. PVD synthesis and transfer into water-based solutions of functionalized gold nanoparticles. *Plasma Processes and Polymers, 6*, pp.888–892.

28. Haute, D.V. and Berlin, J.M., **2017**. Challenges in realizing selectivity for nanoparticle biodistribution and clearance: Lessons from gold nanoparticles. *Therapeutic Delivery, 8*(9), pp.763–774.

29. Del Monte, U., **2009**. Does the cell number 109 still really fit one gram of tumor tissue? *Cell Cycle, 8*(3), pp.505–506.

30. Bailly, A.L., Correard, F., Popov, A., Tselikov, G., Chaspoul, F., Appay, R., Al-Kattan, A., Kabashin, A. V., Braguer, D. and Esteve, M.A., **2019**. In vivo evaluation of safety, biodistribution and pharmacokinetics of laser-synthesized gold nanoparticles. *Scientific Reports, 9*(1), Article No: 12890.

31. Li, B. and Lane, L.A., **2019**. Probing the biological obstacles of nanomedicine with gold nanoparticles. *Wiley Interdisciplinary Reviews Nanomedicine and Nanobiotechnology, 11*(3), Article No: e1542.

32. Taylor, U., Rehbock, C., Streich, C., Rath, D. and Barcikowski, S., **2014**. Rational design of gold nanoparticle toxicology assays: A question of exposure scenario, dose and experimental setup. *Nanomedicine (London, England), 9*(13), pp.1971–1989.

33. Bednarski, M., Dudek, M., Knutelska, J., Nowinski, L., Sapa, J., Zygmunt, M., Nowak, G., Luty-Blocho, M., Wojnicki, M., Fitzner, K. and Tesiorowski, M., **2015**. The influence of the route of administration of gold nanoparticles on their tissue distribution and basic biochemical parameters: In vivo studies. *Pharmacological Reports*, *67*(3), pp.405–409.

34. Alalaiwe, A., Roberts, G., Carpinone, P., Munson, J. and Roberts, S., **2017**. Influence of PEG coating on the oral bioavailability of gold nanoparticles in rats. *Drug Delivery*, *24*(1), pp.591–598.

35. Campbell, J.L., Sorelle, E.D., Ilovich, O., Liba, O., James, M.L., Qiu, Z., Perez, V., Chan, C.T., De La Zerda, A. and Zavaleta, C., **2017**. Multimodal assessment of SERS nanoparticle biodistribution post ingestion reveals new potential for clinical translation of Raman imaging. *Biomaterials*, *135*, pp.42–52.

36. Rambanapasi, C., Barnard, N., Grobler, A., Buntting, H., Sonopo, M., Jansen, D., Jordaan, A., Steyn, H. and Zeevaart, J.R., **2015**. Dual radiolabeling as a technique to track nanocarriers: The case of gold nanoparticles. *Molecules*, *20*(7), pp.12863–12879.

37. Arvizo, R.R., Miranda, O.R., Moyano, D.F., Walden, C.A., Giri, K., Bhattacharya, R., Robertson, J.D., Rotello, V.M., Reid, J.M. and Mukherjee, P., **2011**. Modulating pharmacokinetics, tumor uptake and biodistribution by engineered nanoparticles. *PloS One*, *6*(9), Article No: e24374.

38. Sadauskas, E., Wallin, H., Stoltenberg, M., Vogel, U., Doering, P., Larsen, A. and Danscher, G., **2007**. Kupffer cells are central in the removal of nanoparticles from the organism. *Particle and Fibre Toxicology*, *4*, Article No: 10.

39. Chen, C.C., Li, J.J., Guo, N.H., Chang, D.Y., Wang, C.Y., Chen, J.T., Lin, W.J., Chi, K.H., Lee, Y.J., Liu, R.S., Chen, C.L. and Wang, H.E., **2019**. Evaluation of the biological behavior of a gold nanocore-encapsulated human serum albumin nanoparticle (Au@HSANP) in a CT-26 tumor/ascites mouse model after intravenous/intraperitoneal administration. *International Journal of Molecular Sciences*, *20*(1), Article No: 217.

40. Morales-Avila, E., Ferro-Flores, G., Ocampo-Garcia, B.E., De Leon-Rodriguez, L.M., Santos-Cuevas, C.L., Garcia-Becerra, R., Medina, L.A. and Gomez-Olivan, L., **2011**. Multimeric system of 99mTc-labeled gold nanoparticles conjugated to c[RGDfK(C)] for molecular imaging of tumor alpha(v)beta(3) expression. *Bioconjugate Chemistry*, *22*(5), pp.913–922.

41. Lee, S.B., Yoon, G., Lee, S.W., Jeong, S.Y., Ahn, B.C., Lim, D.K., Lee, J. and Jeon, Y.H., **2016**. Combined positron emission tomography and cerenkov luminescence imaging of sentinel lymph nodes using PEGylated radionuclide-embedded gold nanoparticles. *Small (Weinheim an der Bergstrasse Germany)*, *12*(35), pp.4894–4901.

42. Kudgus, R.A., Walden, C.A., McGovern, R.M., Reid, J.M., Robertson, J.D. and Mukherjee, P., **2014**. Tuning pharmacokinetics and biodistribution of a targeted drug delivery system through incorporation of a passive targeting component. *Scientific Reports*, *4*, Article No: 5669.

43. Kao, H.W., Lin, Y.Y., Chen, C.C., Chi, K.H., Tien, D.C., Hsia, C.C., Lin, W.J., Chen, F.D., Lin, M.H. and Wang, H.E., **2014**. Biological characterization of cetuximab-conjugated gold nanoparticles in a tumor animal model. *Nanotechnology*, *25*(29), Article No: 295102.

44. Niidome, T., Yamagata, M., Okamoto, Y., Akiyama, Y., Takahashi, H., Kawano, T., Katayama, Y. and Niidome, Y., **2006**. PEG-modified gold nanorods with a stealth character for in vivo applications. *Journal of Controlled Release: Official Journal of the Controlled Release Society*, *114*(3), pp.343–347.

45. Huang, K., Ma, H., Liu, J., Huo, S., Kumar, A., Wei, T., Zhang, X., Jin, S., Gan, Y., Wang, P.C., He, S. and Liang, X.J., **2012**. Size-dependent localization and penetration of ultrasmall gold nanoparticles in cancer cells, multicellular spheroids, and tumors in vivo. *ACS Nano*, *6*(5), pp.4483–4493.

46. Huo, S., Ma, H., Huang, K., Liu, J., Wei, T., Jin, S., Zhang, J., He, S. and Liang, X.J., **2013**. Superior penetration and retention behavior of 50 nm gold nanoparticles in tumors. *Cancer Research*, *73*(1), pp.319–330.

47. Akiyama, Y., Mori, T., Katayama, Y. and Niidome, T., **2009**. The effects of PEG grafting level and injection dose on gold nanorod biodistribution in the tumor-bearing mice. *Journal of Controlled Release: Official Journal of the Controlled Release Society*, *139*(1), pp.81–84.

48. Lipka, J., Semmler-Behnke, M., Sperling, R.A., Wenk, A., Takenaka, S., Schleh, C., Kissel, T., Parak, W. J. and Kreyling, W.G., **2010**. Biodistribution of PEG-modified gold nanoparticles following intratracheal instillation and intravenous injection. *Biomaterials*, *31*(25), pp.6574–6581.

49. You, J., Zhou, J., Zhou, M., Liu, Y., Robertson, J.D., Liang, D., Van Pelt, C. and Li, C., **2014**. Pharmacokinetics, clearance, and biosafety of polyethylene glycol-coated hollow gold nanospheres. *Particle and Fibre Toxicology*, *11*, Article No: 26.

50. Bogdanov Jr., A.A., Gupta, S., Koshkina, N., Corr, S.J., Zhang, S., Curley, S.A. and Han, G., **2015**. Gold nanoparticles stabilized with MPEG-grafted poly(l-lysine): In vitro and in vivo evaluation of a potential theranostic agent. *Bioconjugate Chemistry*, *26*(1), pp.39–50.

51. Hirn, S., Semmler-Behnke, M., Schleh, C., Wenk, A., Lipka, J., Schäffler, M., Takenaka, S., Möller, W., Schmid, G., Simon, U. and Kreyling, W.G., **2011**. Particle size-dependent and surface charge-dependent biodistribution of gold nanoparticles after intravenous administration. *European Journal of Pharmaceutics and Biopharmaceutics*, *77*(3), pp.407–416.

52. Sonavane, G., Tomoda, K. and Makino, K., **2008**. Biodistribution of colloidal gold nanoparticles after intravenous administration: Effect of particle size. *Colloids and Surfaces B: Biointerfaces*, *66*(2), pp.274–280.

53. De Jong, W.H., Hagens, W.I., Krystek, P., Burger, M.C., Sips, A.J. and Geertsma, R.E., **2008**. Particle size-dependent organ distribution of gold nanoparticles after intravenous administration. *Biomaterials*, *29*(12), pp.1912–1919.

54. Li, X., Hu, Z., Ma, J., Wang, X., Zhang, Y., Wang, W. and Yuan, Z., **2018**. The systematic evaluation of size-dependent toxicity and multi-time biodistribution of gold nanoparticles. *Colloids and Surfaces B: Biointerfaces*, *167*, pp.260–266.

55. Alfranca, G., Beola, L., Liu, Y., Gutierrez, L., Zhang, A., Artiga, A., Cui, D. and De La Fuente, J.M., **2019**. In vivo comparison of the biodistribution and long-term fate of colloids-gold nanoprisms and nanorods-with minimum surface modification. *Nanomedicine (London, England)*, *14*(23), pp.3035–3055.

56. Sadauskas, E., Danscher, G., Stoltenberg, M., Vogel, U., Larsen, A. and Wallin, H., **2009**. Protracted elimination of gold nanoparticles from mouse liver. *Nanomedicine: Nanotechnology, Biology, and Medicine*, *5*(2), pp.162–169.

57. Aborig, M., Malik, P.R.V., Nambiar, S., Chelle, P., Darko, J., Mutsaers, A., Edginton, A.N., Fleck, A., Osei, E. and Wettig, S., **2019**. Biodistribution and physiologically-based pharmacokinetic modeling of gold nanoparticles in mice with interspecies extrapolation. *Pharmaceutics*, *11*(4), Article No: 179.

58. Poon, W., Zhang, Y.N., Ouyang, B., Kingston, B.R., Wu, J.L.Y., Wilhelm, S. and Chan, W.C.W., **2019**. Elimination pathways of nanoparticles. *ACS Nano*, *13*(5), pp.5785–5798.

59. Manshian, B.B., Pokhrel, S., Madler, L. and Soenen, S.J., **2018**. The impact of nanoparticle-driven lysosomal alkalinization on cellular functionality. *J. Nanobiotechnology*, *16*(1), Article No: 85.

60. McGill, M.R., Williams, C.D., Xie, Y., Ramachandran, A. and Jaeschke, H., **2012**. Acetaminophen-induced liver injury in rats and mice: Comparison of protein adducts, mitochondrial dysfunction, and oxidative stress in the mechanism of toxicity. *Toxicology and Applied Pharmacology*, *264*(3), pp.387–394.

61. James, L.P., McCullough, S.S., Lamps, L.W. and Hinson, J.A., **2003**. Effect of N-acetylcysteine on acetaminophen toxicity in mice: Relationship to reactive nitrogen and cytokine formation. *Toxicological Sciences*, *75*(2), pp.458–467.

62. Rambanapasi, C., Zeevaart, J.R., Buntting, H., Bester, C., Kotze, D., Hayeshi, R. and Grobler, A., **2016**. Bioaccumulation and subchronic toxicity of 14 nm gold nanoparticles in rats. *Molecules*, *21*(6), Article No: 763.

63. Lopez-Chaves, C., Soto-Alvaredo, J., Montes-Bayon, M., Bettmer, J., Llopis, J. and Sanchez-Gonzalez, C., **2018**. Gold nanoparticles: Distribution, bioaccumulation and toxicity. In vitro and in vivo studies. *Nanomedicine: Nanotechnology, Biology, and Medicine, 14*(1), pp.1–12.

64. Dam, D.H., Culver, K.S., Kandela, I., Lee, R.C., Chandra, K., Lee, H., Mantis, C., Ugolkov, A., Mazar, A.P. and Odom, T.W., **2015**. Biodistribution and in vivo toxicity of aptamer-loaded gold nanostars. *Nanomedicine: Nanotechnology, Biology, and Medicine*, *11*(3), pp.671–679.

65. Le, Q.L., Linh Do, T.P., Nguyen, H.P.U., Dang, V.P. and Nguyen, Q.H., **2014**. Biodistribution of gold nanoparticles synthesized by γ-irradiation after intravenous administration in mice. *Advances in Natural Sciences: Nanoscience and Nanotechnology*, *5*(2), Article No: 025009.

66. Eggers, K.M., Kempf, T., Lind, L., Sundstrom, J., Wallentin, L., Wollert, K.C. and Siegbahn, A., **2012**. Relations of growth-differentiation factor-15 to biomarkers reflecting vascular pathologies in a population-based sample of elderly subjects. *Scandinavian Journal of Clinical and Laboratory Investigation*, *72*(1), pp.45–51.

67. Ibrahim, K.E., Bakhiet, A.O., Awadalla, M.E. and Khan, H.A., **2018**. A priming dose protects against gold nanoparticles-induced proinflammatory cytokines mRNA expression in mice. *Nanomedicine (London, England), 13*(3), pp.313–323.

68. Simpson, C.A., Salleng, K.J., Cliffel, D.E. and Feldheim, D.L., **2013**. In vivo toxicity, biodistribution, and clearance of glutathione-coated gold nanoparticles. *Nanomedicine: Nanotechnology, Biology, and Medicine, 9*(2), pp.257–263.

69. Uchiyama, M.K., Deda, D.K., Rodrigues, S.F., Drewes, C.C., Bolonheis, S.M., Kiyohara, P.K., Toledo, S.P., Colli, W., Araki, K. and Farsky, S.H., **2014**. In vivo and in vitro toxicity and anti-inflammatory properties of gold nanoparticle bioconjugates to the vascular system. *Toxicological Sciences*, *142*(2), pp.497–507.

70. Ibrahim, K.E., Al-Mutary, M.G., Bakhiet, A.O. and Khan, H.A., **2018**. Histopathology of the liver, kidney, and spleen of mice exposed to gold nanoparticles. *Molecules*, *23*(8), Article No: 1848.

71. Victora, G.D., **2014**. SnapShot: The germinal center reaction. *Cell*, *159*(3), pp.700–701.

72. Zhang, X.D., Wu, H.Y., Wu, D., Wang, Y.Y., Chang, J.H., Zhai, Z.B., Meng, A.M., Liu, P.X., Zhang, L.A. and Fan, F.Y., **2010**. Toxicologic effects of gold nanoparticles in vivo by different administration routes. *International Journal of Nanomedicine*, *5*, pp.771–781.

73. Adewale, O.B., Davids, H., Cairncross, L. and Roux, S., **2019**. Toxicological behavior of gold nanoparticles on various models: Influence of physicochemical properties and other factors. *International Journal of Toxicology*, *38*(5), pp.357–384.

74. Arvizo, R.R., Miranda, O.R., Thompson, M.A., Pabelick, C.M., Bhattacharya, R., Robertson, J.D., Rotello, V.M., Prakash, Y.S. and Mukherjee, P., **2010**. Effect of nanoparticle surface charge at the plasma membrane and beyond. *Nano Letters*, *10*(7), pp.2543–2548.

75. Harper, S.L., Carriere, J.L., Miller, J.M., Hutchison, J.E., Maddux, B.L. and Tanguay, R.L., **2011**. Systematic evaluation of nanomaterial toxicity: Utility of standardized materials and rapid assays. *ACS Nano*, *5*(6), pp.4688–4697.

76. Puvanakrishnan, P., Park, J., Chatterjee, D., Krishnan, S. and Tunnell, J.W., **2012**. In vivo tumor targeting of gold nanoparticles: Effect of particle type and dosing strategy. *International Journal of Nanomedicine*, *7*, pp.1251–1258.

77. Weaver, J.L., Tobin, G.A., Ingle, T., Bancos, S., Stevens, D., Rouse, R., Howard, K.E., Goodwin, D., Knapton, A., Li, X., Shea, K., Stewart, S., Xu, L., Goering, P.L., Zhang, Q., Howard, P.C., Collins, J., Khan, S., Sung, K. and Tyner, K.M., **2017**. Evaluating the potential of gold, silver, and silica nanoparticles to saturate mononuclear phagocytic system tissues under repeat dosing conditions. *Particle and Fibre Toxicology*, *14*(1), Article No: 25.